SCIENTIFIC REPORTS

OPEN

Anomalous temperature-dependent spin-valley polarization in monolayer WS$_2$

A.T. Hanbicki[1], G. Kioseoglou[2,3], M. Currie[4], C. Stephen Hellberg[1], K.M. McCreary[1], A.L. Friedman[1] & B.T. Jonker[1]

Single layers of transition metal dichalcogenides (TMDs) are direct gap semiconductors with nondegenerate valley indices. An intriguing possibility for these materials is the use of their valley index as an alternate state variable. Several limitations to such a utility include strong intervalley scattering, as well as multiparticle interactions leading to multiple emission channels. We prepare single-layer WS$_2$ films such that the photoluminescence is from either the neutral or charged exciton (trion). After excitation with circularly polarized light, the neutral exciton emission has zero polarization. However, the trion emission has a large polarization (28%) at room temperature. The trion emission also has a unique, non-monotonic temperature dependence that is a consequence of the multiparticle nature of the trion. This temperature dependence enables us to determine that intervalley scattering, electron-hole radiative recombination, and Auger processes are the dominant mechanisms at work in this system. Because this dependence involves trion systems, one can use gate voltages to modulate the polarization (or intensity) emitted from TMD structures.

In low-dimensional, hexagonal-lattice structures there are two degenerate, yet inequivalent K-points in the Brillouin zone, labeled K and K'. These high symmetry points are at the edge of the Brillouin zone and are usually local extrema: a local maximum in the valence band and a local minimum (or valley) in the conduction band. Much like electron charge or spin, this valley index can be used as a state variable to control the operation of an electronic device[1–3]. Single layers of transition metal dichalcogenides (TMDs) are semiconductors with a direct gap at the K-points, and are well known for their potential as valleytronic materials[4–6]. One way to access the valleytronic functionality in these materials is via spin-valley coupling. Because of strong orbital hybridization and time-reversal symmetry, the valence band maximum in each valley has only one spin state (the conduction band is nearly spin degenerate), giving these materials unique optical selection rules[4–7]. It is therefore possible to selectively populate and interrogate the different valleys, K or K', using circularly polarized light. Past work exploring the spin-valley coupling with optical techniques[4–6,8–13], and some recent progress coupling these optical techniques with transport measurements hints at possible applications for these materials[14,15].

Optical excitation creates electron-hole pairs that can bind to form quasiparticles known as excitons. When single-layer TMDs are excited with circularly polarized light, excitons are created in a single valley. The radiative decay of excitons within this valley subsequently produces circularly polarized light due to the optical selection rules. Therefore, measuring the circular polarization of electroluminescence or photoluminescence (PL) provides a direct way to monitor valley populations. Populations are altered by intervalley scattering, a process that is enabled by either the Coulomb interaction or phonons[10,12,16]. At high temperatures or high photoexcitation energy, large phonon populations can readily couple the valleys, reducing valley specific populations. Because of this strong intervalley coupling, exciton polarization is often only seen in systems measured at low temperature or near resonant pumping conditions[6,8–10].

In addition to the excitonic emission, photoluminescence spectra from TMDs have a plethora of other features that speak to the complexity and richness of these systems[6,11,17,18]. For instance, a third carrier (electron or hole) can bind to the exciton complex creating a charged exciton, or trion, with an emission energy lower than the exciton.

[1]Materials Science and Technology Division, Naval Research Laboratory, Washington, DC 20375. [2]University of Crete, Heraklion Crete, 71003, Greece. [3]Institute of Electronic Structure and Laser (IESL), Foundation for Research and Technology Hellas (FORTH), Heraklion Crete, 71110, Greece. [4]Optical Sciences Division, Naval Research Laboratory, Washington, DC 20375. Correspondence and requests for materials should be addressed to A.T.H. (email: hanbicki@nrl.navy.mil)

Unfortunately, this adds a confounding dimension to the interpretation of the results, and the utility of TMDs as valleytronic materials because the origin of many of the emission features is unknown and they are difficult to create reproducibly. For instance, in WSe$_2$ varying degrees of polarization have been measured for various emission channels of unknown origin[11].

Here we show that we can isolate two distinct initial states in naturally n-doped, single layer WS$_2$: a neutral exciton and a trion. When excited with circularly polarized light, the PL of the neutral exciton has zero circular polarization at room temperature. However, the trion has a polarization as high as 28%. Even with excitation energies far from the resonant condition (>300 meV), the trion emission maintains some circular polarization. The trion emission polarization also displays a unique temperature dependence. There is a pronounced increase in polarization at an intermediate temperature with a broad peak of 42% in the temperature range 175–250 K. We show that non-monotonic temperature dependence is a consequence of the multiparticle nature of the trion and propose a second recombination channel that is more readily available in 3-particle systems. This enables us to determine the dominant mechanisms at work in this sub-system and to speculate on the suitability of this material for future valleytronic applications.

Results

Initial Conditions. Samples used here include monolayer flakes mechanically exfoliated from bulk WS$_2$ single crystals as well as large area layers of WS$_2$ grown by chemical vapor deposition. A microscope image of a representative exfoliated sample is shown in Fig. 1a, and the Raman spectrum of the monolayer is shown in Fig. 1b. The energy separation of the two Raman modes and accompanying PL confirm the single layer nature of our sample. Additional details of sample preparation are found in the methods and supplementary information. The data presented below is from this representative sample, but all of the results were reproduced on several monolayer samples of independent origin.

Once the single layer regions are identified, we measured the normalized reflectivity (Fig. 1c), and the energy-resolved PL (Fig. 1d) at 300 K. For WS$_2$, these spectra depend crucially on the preparation of the sample. In Fig. 1c,d, the as-exfoliated spectra (thin, blue lines) are distinct from those measured after purposeful preparation in vacuum (thick, red lines). The sample preparation[19] consists of rastering a 532 nm laser (2 mW power and ~1 μm spot size) across the entire flake while in a 10^{-6} Torr vacuum to desorb weakly bound contaminants[20,21]. As can be seen in Fig. 1c,d, after treatment a peak emerges 33 meV below the peak observed in the as-exfoliated sample. The n-type conductivity measured by transport increases significantly after treatment as well. More details of this effect are described in the methods, supplemental materials, and elsewhere[19].

When excess electrons are present, the neutral exciton (X^0) can capture an electron to form a negatively charged exciton, or trion (X$^-$). In GaAs, for instance[22], at a critical electron density there is a sharp transfer of oscillator strength from X^0 to X$^-$, and eventually X^0 is completely quenched. A similar behavior is seen here. We attribute the high-energy feature in Fig. 1c,d to X^0 (thin, blue line), and the low-energy feature to X$^-$ (thick, red line). An identical assignment was made in reference[21].

The separation of the X^0 and X$^-$ peaks in the reflectivity spectra is 33 meV. This energy is consistent with the binding energy of the charged exciton measured for MoS$_2$[17] and MoSe$_2$[18], and predicted for all of the monolayer transition metal dichalcogenides[23]. In our PL measurement, the X$^-$ energy is shifted to a lower energy than observed in reflectivity and the width is larger than the neutral exciton. The energy shift is commonly seen for trions and can be attributed to a bandgap renormalization due to the electron density[22]. Furthermore, scattering by electrons is found to be an efficient process, even for low electron densities. Therefore, the trion linewidth due to electron scattering is larger than that of the neutral exciton because of the larger contribution from the dissociation process as well as processes such as inhomogeneous broadening. Finally, in the TMD systems the binding energy of the exciton[24–28] and the trion[18,23] are much larger than traditional materials like GaAs[29]. Therefore, we expect and confirm that the trion is stabilized to a much higher temperature, *i.e.* the trion emission remains at room temperature.

Measuring the Polarization. From Fig. 1c,d it is clear that we are able to isolate the X^0 and X$^-$ peaks by conditioning the sample. This allows us to reproducibly prepare the surface so that trends in temperature, excitation energy, and circular polarization can be reliably measured for each[19]. Figure 2 shows the PL of WS$_2$ from the neutral exciton (Fig. 2a), and from the trion, (Fig. 2b) at room temperature (left panels) and 4 K (right panels). The spectra were obtained with a circularly polarized excitation source with positive helicity ($\sigma+$) and excitation energy of 2.087 eV (594 nm laser). The resulting emission was analyzed for positive ($\sigma+$, solid red line) and negative helicity ($\sigma-$, open, blue circles). The polarization is defined as $P = [I(\sigma+) - I(\sigma-)]/[I(\sigma+) + I(\sigma-)]$, where $I(\sigma\pm)$ is the emission intensity analyzed for positive (negative) helicity. The most notable feature of these spectra is that, even at room temperature, the trion has a very large circular polarization, $P = 28\%$. This is in marked contrast to the free exciton, which has 0% polarization at room temperature using the same excitation conditions. The results at low temperature are also unexpected. The neutral exciton has a polarization roughly half that of the trion, and the trion polarization is about the same at low temperature as it is at room temperature. We measured polarization when both the exciton and trion are present to verify that this result is not a consequence of sample preparation (see supplementary information).

To understand the origin of the large room temperature polarization of the trion, as well as the relatively meager polarization at low temperature we measured the helicity-resolved PL from prepared WS$_2$ as a function of temperature for 10 different excitation energies. Figure 3a,b are representative sets of data taken with positive helicity excitation sources of 2.087 eV (594 nm), and 2.331 eV (532 nm), respectively. For each excitation energy, we obtained data from 4 K to 300 K. In these figures the spectra are offset for clarity. Plots of spectra from all ten excitation energies are provided in the supplemental information.
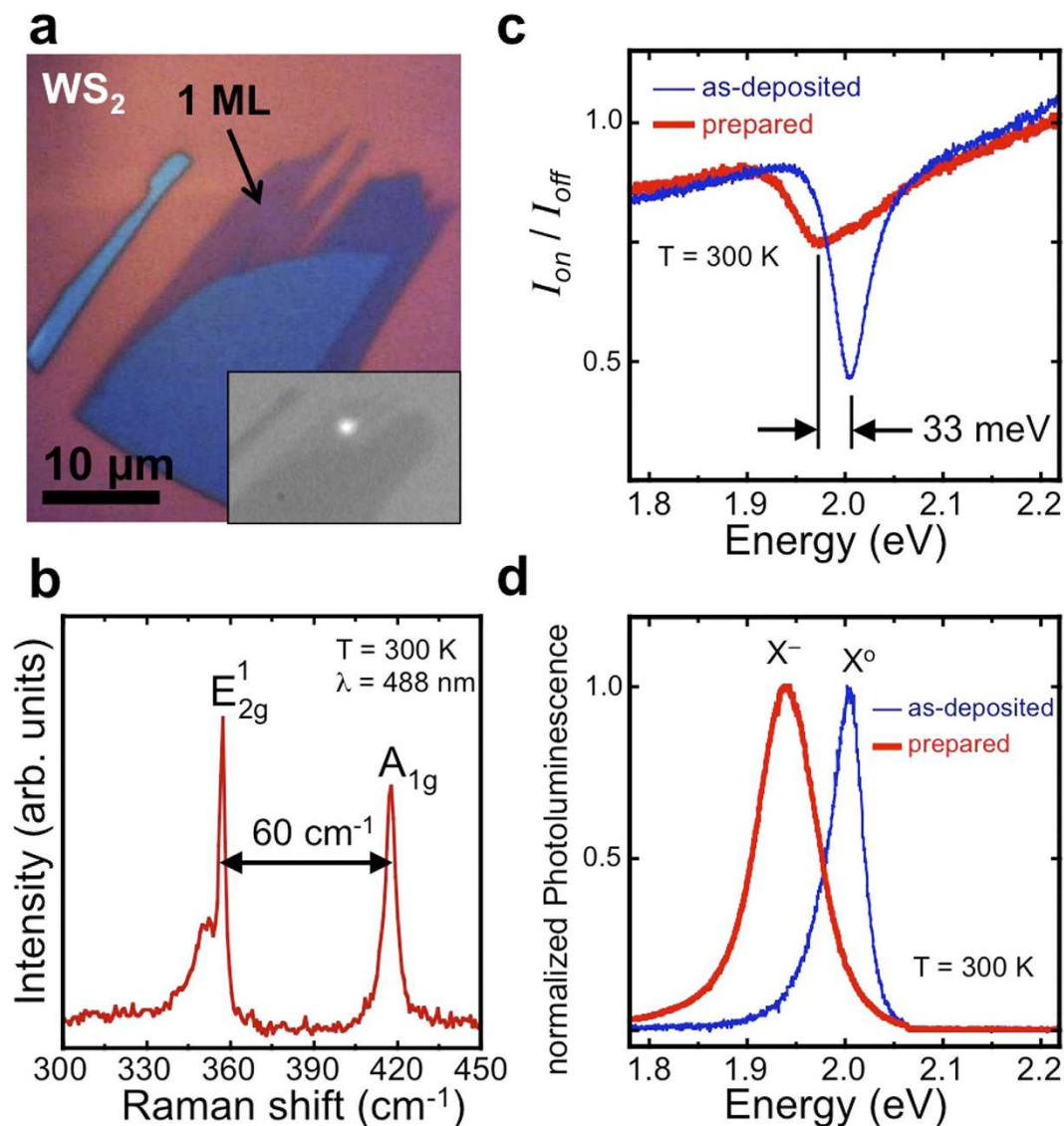
Figure 1. Monolayer WS$_2$ characterization. (**a**) Optical microscope images of representative WS$_2$ flake with the monolayer region indicated. The inset shows the photoluminescence from the flake at room temperature to illustrate the spot size. (**b**) Raman spectrum of the monolayer regions taken at 300 K with an excitation energy of 488 nm. The splitting of the in-plane E$_{2g}^1$ mode and the out-of-plane A$_{1g}$ mode are characteristic of a single layer. Normalized (**c**) reflectivity and (**d**) photoluminescence spectra taken at room temperature for the as-deposited sample in air (thin, blue line) and the sample in vacuum prepared as described in the text (thick, red line).

Analyzing the Polarization. A compilation of the raw data for the trion polarization is displayed in Fig. 4. In this figure, the polarization is plotted as both a function of temperature for all the excitation energies used (Fig. 4a) and as a function of excess energy (Fig. 4b), which is the difference between the excitation and emission energies, $\Delta E = E_{\text{excitation}} - E_{\text{emission}}$[30]. There are several interesting and novel features in these data.

First, the trion polarization at room temperature is 28% for excitation 150 meV above the emission energy. As the temperature increases or the excitation energy increases, phonons become available and the polarization decreases rapidly because of intervalley scattering[10]. Several contradictory room temperature polarization measurements have been reported for MoS$_2$[6,9]. Mak *et al.* report zero polarization at room temperature, while Sallen, *et al.* report 40% polarization at room temperature. In both cases, they used excitation energies 100 meV higher than the emission energy. To our knowledge, no room-temperature polarization has been reported for any other TMD.

Second, at low temperature (4 K), the polarization never exceeds 25%, even with an excitation energy only 100 meV above the emission energy. When the excitation energy is less than 2 LA phonons above the emission energy, there is insufficient energy to excite the phonons necessary for intervalley scattering, and the polarization should be 100%[10]. For WS$_2$, 2 LA is 46 meV[31,32], for MoS$_2$, it is 60 meV[31]. Although we are exciting the WS$_2$ near the emission energy, we observe a relatively modest polarization of 25% at 4 K. This starkly contrasts with the very high polarizations reported at low temperature for MoS$_2$[6,9].
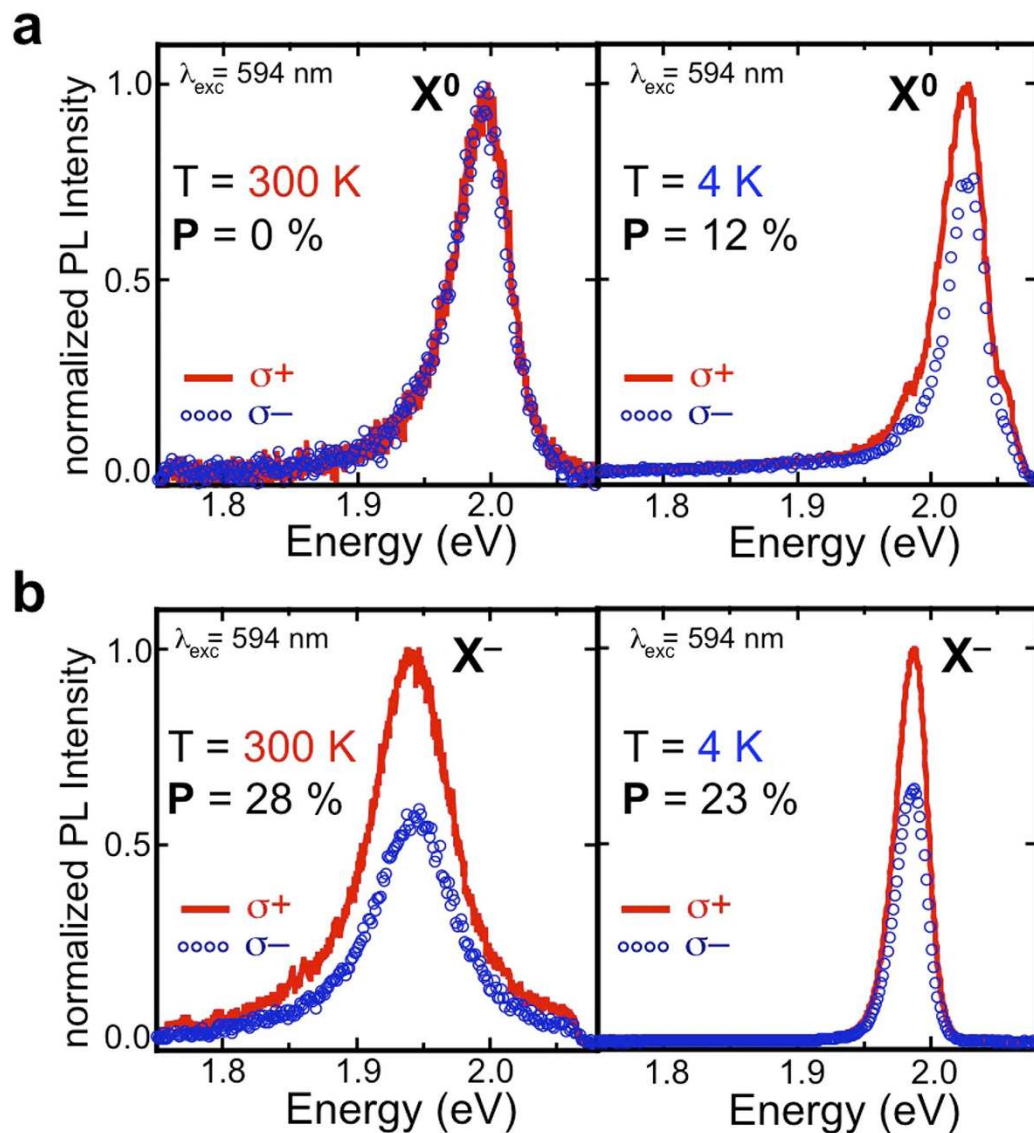
Figure 2. Polarization of monolayer WS$_2$ neutral and charged exciton. Photoluminescence analyzed for positive ($\sigma+$: solid, red trace) and negative ($\sigma-$: blue, open circles) helicity of the (**a**) neutral exciton and (**b**) charged exciton. Spectra taken in the left (right) panels are taken at room temperature (4 K). The excitation was with an energy of 2.087 eV and positive helicity.

Perhaps the most intriguing feature of these data is that the polarization *increases* significantly with increasing temperature, even when exciting the system with an energy 300 meV above the emission energy. Such an increase in the polarization at intermediate temperature has not been observed before, and we propose that this is a unique consequence of the emission originating from a 3-particle entity (the trion) rather than from a simple exciton. When the excitation energy is 350 meV higher than the emission energy (i.e. laser wavelengths <532 nm), the polarization decreases smoothly as a function of temperature as observed in other TMD monolayers[10].

An alternative way of presenting the data is to plot the circular polarization of the trion as a function of the energy difference between the laser excitation energy and the PL emission line (Fig. 4b). The quantity ΔE depends both on the excitation energy and the temperature due to the dependence of the emission energy on temperature. The behavior of the polarization vs. ΔE in WS$_2$ is quite different than that observed in MoS$_2$[10,13] and MoSe$_2$[30]. As can be seen in Fig. 4b, the dependence of the polarization on ΔE collapses onto two branches. The lower branch (closed, blue circles) consists of all the data taken at 125 K and below. The upper branch (open, red circles) is the higher temperature data. The transition from the lower branch to the upper branch occurs gradually from 125 K to 175 K, as is shown in the inset. Here we will not attempt to explain the overall temperature dependence, but rather the jump from the low temperature branch to the high temperature branch.

To elucidate the mechanisms leading to the anomalous temperature dependence, we focus on the data collected using the lowest excitation energies, *i.e.* near-resonant excitation (within 150 meV of the exciton emission). Figure 5a shows the temperature dependence of the circular polarization using the 2.087 eV and 2.109 eV sources
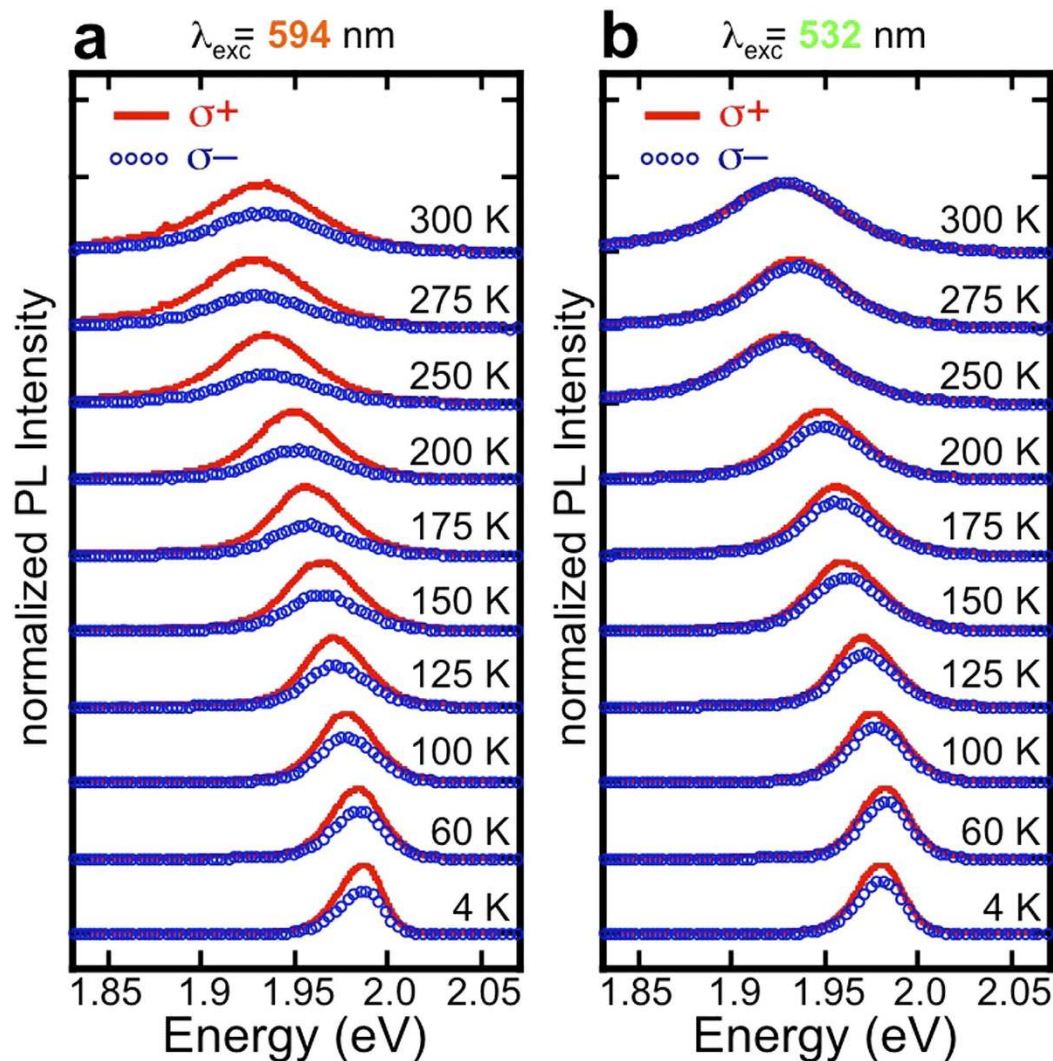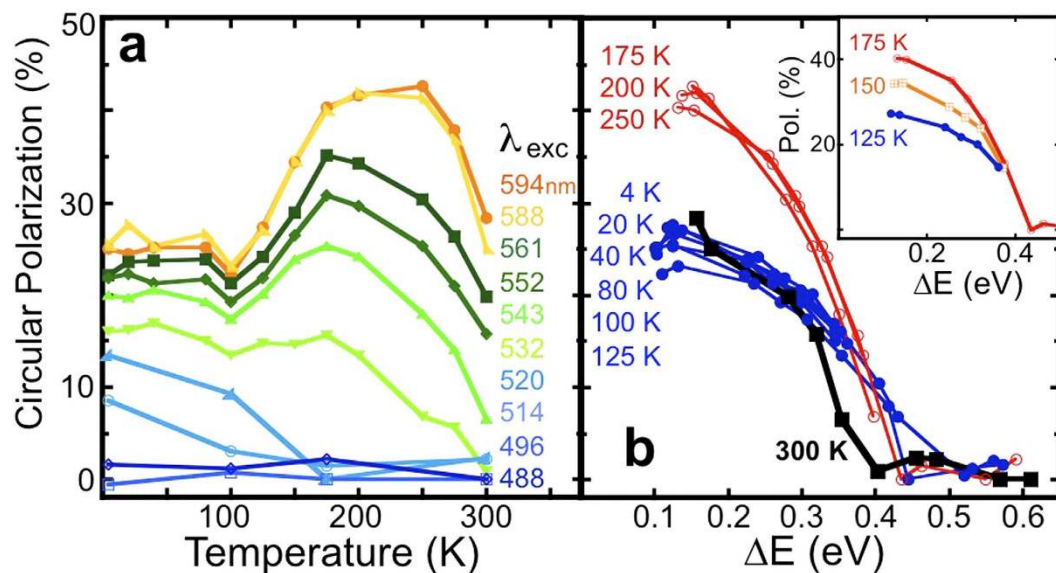
Figure 4. Temperature and excitation energy dependence of the monolayer WS$_2$ charged exciton polarization. Summary of the circular polarization (**a**) as a function of temperature for each excitation wavelength used, and (**b**) as a function of excess energy, ΔE. Polarization is calculated from the spectra presented in Fig. 3 and S2.

$$P = \frac{P_0}{(1 + 2 \cdot \beta/\alpha)}. \tag{1}$$

Here P_0 is the initial polarization of the system, α is the exciton radiative recombination rate, and β is the rate of spin relaxation. Note that $\alpha = 1/\tau_r$ and $\beta = 1/\tau_s$ where τ_r is the recombination time, and τ_s is the spin relaxation time. Because of the unique selection rules in this system[4–7], spin relaxation is related to the intervalley scattering rate. To first order, we consider the spin relaxation time equivalent to the intervalley scattering time. Also, although the temperature dependence of P_0 can be rather complicated as a function of excitation energy[33], again to first order we do not consider it. A schematic definition of these processes as well as a full derivation of this equation is presented in the supplemental information. Some insight into the physical processes of this system is obtained when we consider the relation of these characteristic rates and times.

At low temperature, the exciton recombination rate, α, is simply the light-emitting electron-hole recombination event in a single valley. The intervalley relaxation, β, is the exciton spin flip-flop where an exciton scatters from one valley to the other[6,12,34]. The intervalley scattering process is fast if the exciton has a large center of mass momentum, and slower if the exciton is close to the ground state momentum[11,35]. For excitons generated by photons far from resonance, *i.e.* with high energy, we expect a large initial center-of-mass momentum, which will be reduced as they relax. Capturing an electron to form a trion will also quickly reduce the momentum. Since we are exciting the system with circularly polarized light, the initial polarization of the system is expected to be very high, i.e. $P_0 \rightarrow 100\%$. A polarization, P, considerably less than this initial polarization means the intervalley relaxation, β, must be faster than the exciton recombination rate, α, and/or the initial polarization, P_0, could somehow be reduced, according to equation (1). Our observed trion polarization of 25% at low temperature means the ratio $\tau_r/\tau_s = \beta/\alpha$ is 1.5, assuming that the initial polarization is 100%. This initial polarization is likely reduced, however, since we are measuring the trion polarization. As is seen in Fig. 2, the polarization of the neutral exciton is roughly half that of the trion at low temperatures. Since the trion forms via excitons capturing electrons, any relaxation prior to trion formation will reduce P_0 for the trion. Indeed, if P_0 is 50%, the ratio β/α is 0.5, still the same order of magnitude. Recombination lifetimes on the order of 1~5 psec have been measured in other TMDs[36], suggesting that the intervalley scattering lifetime must be of the same picosecond timescale.

It is also important to include non-radiative recombination channels for the trion, such as Auger processes. Auger recombination has been found to be strong in MoS$_2$ monolayers[37,38]. In this three-particle process, an electron and hole recombine non-radiatively, transferring energy to a third electron (or hole), which moves to a higher energy level[39]. The Auger recombination rate of trions has been observed to increase with increasing temperature in nanocrystals[40], and in MoS$_2$ monolayers an activation energy of 22 meV (255 K) has been reported[41]. Incorporating non-radiative recombination into the rate equation analysis yields a polarization

$$P = \frac{P_0}{(1 + 2 \cdot \beta/(\alpha + A))} \tag{2}$$

where the rate A includes all non-radiative paths, including Auger recombination. The addition of non-radiative recombination channels reduces the light emission intensity, yielding
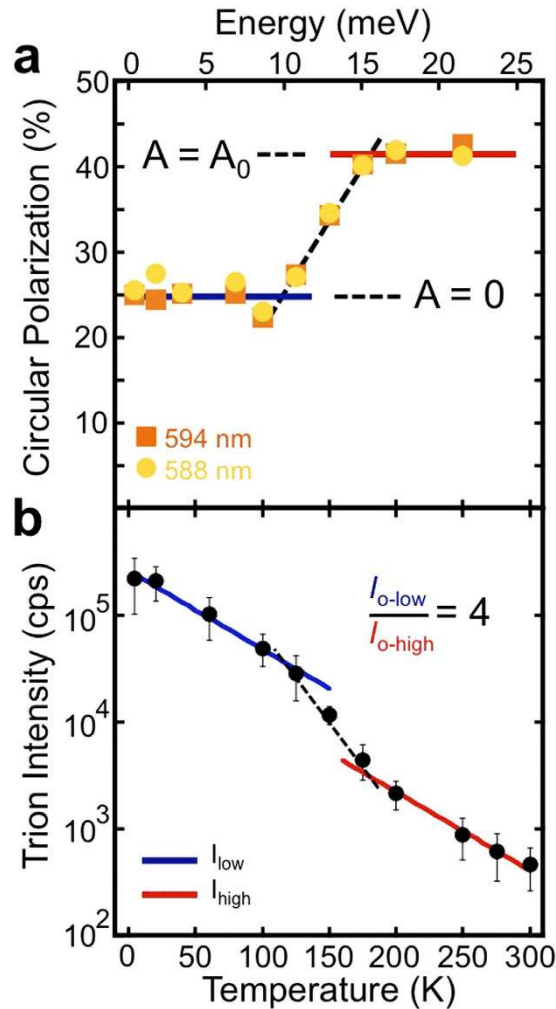
Figure 5. Temperature dependent behavior of circular polarization and trion intensity. (a) Temperature dependence of the circular polarization for the two lowest excitation energies used (594 and 588 nm). The solid line is a guide to the eye to illustrate the two-level behavior. The Auger recombination rate, A, described in the text, is zero for the lower level of polarization and becomes non-zero after a certain temperature. **(b)** Intensity of the trion peak as a function of temperature. The solid lines through the data are fits assuming a simple exponential decrease in intensity with a low and high temperature prefactor.

$$I_{tot} = I(\sigma +) + I(\sigma-) = \frac{\alpha}{(\alpha + A)}. \tag{3}$$

Again, $I(\sigma\pm)$ is the measured intensity of positive (negative) helicity light. It is clear that an increase in the Auger recombination rate, A, will simultaneously cause a drop in the measured intensity along with an increase in the measured polarization. Indeed, as is shown in Fig. 5b, there is a significant drop in emission intensity from 125 K to 175 K, the same temperature range where there is an increase in polarization. More quantitatively, the temperature dependence of the intensity can be fit with a single exponential function, $I = I_o\, e^{-cT}$ where c is a constant. We use this simple phenomenological exponential factor not to imply any particular physical process, but rather to highlight the specific change in the data at the temperatures of interest. Using the same exponential decay constant, c, and only changing the intensity prefactor, I_o, the low-temperature fit (solid blue line) and high-temperature fit (solid red line) are related by $I_{o-low}/I_{o-high} = 4$. This ratio suggests the Auger rate is 3 times larger than the radiative recombination rate based on equation (3). Therefore, in this model, if $A = 3\alpha$, $\beta = 0.5\alpha$, and $P_0 = 50\%$, then at low temperature the polarization should be 25% and at high temperature it should jump to 40%. These values sufficiently reproduce the trends observed in our data to suggest the Auger process significantly affects the high temperature behavior of WS$_2$ trion system. There are many other possible channels that could contribute to radiative and non-radiative decay. One example is trapping from defect states[42]. However, most of these channels have monotonic temperature dependence and therefore cannot explain our data.

In summary, we have prepared naturally n-doped, single-layer WS$_2$ such that the emitted PL is from either the neutral exciton or the trion. The measured degree of circular polarization shows that while the neutral exciton has zero polarization at room temperature, the trion exhibits a polarization of 28%. The trion polarization also exhibits

a distinct, non-monotonic behavior with temperature – the polarization has a broad peak of 42% between 175 and 250 K. To explain this anomalous behavior, we develop a model that includes a non-radiative recombination mechanism. Intervalley scattering, electron-hole radiative recombination, and a 3-particle Auger process are the dominant mechanisms at work in this system and account for the novel temperature dependence. Because this dependence is unique to the trion systems, one can use, for example, a gate voltage to switch the polarization (or intensity) emitted from these TMD structures. The circular polarization modulation could be used to control interactions between chiral materials on a sub-micrometer scale, enabling various valleytronic applications/systems.

Methods

Sample synthesis and isolation.
Three different samples were used in this study: an exfoliated monolayer purchased from 2D semiconductors, a monolayer that we exfoliated from a bulk crystal, and a large-area, single monolayer grown by chemical vapor deposition (CVD). Further details for each sample are given in the supplementary information. Single layer regions are identified and confirmed in several ways. First, we sweep a 1 mW, 532 nm laser over the sample at room temperature. The PL from a WS_2 monolayer is orders-of-magnitude greater than from multilayers. In fact, luminescence from a monolayer is easily seen with a standard charge-coupled device (CCD)camera as is shown in the inset of Fig. 1a. Next, we measure the Raman spectra of the thin, optically active regions (Fig. 1b). An energy separation of 60 cm^{-1} between the in-plane E^1_{2g} and out-of-plane A_{1g} mode is a clear signature of a single layer of WS_2[32].

Sample preparation.
On all samples, exposing the sample to even a low power excitation source will start to modify the photoluminescence spectrum. The trion feature emerges when the sample is under vacuum and $<1\,\mu W$ of laser power is applied to the sample. Therefore, preparation of the sample consisted of rastering a 532 nm laser of 2 mW power and ~1 μm spot size across the entire flake while in a 10^{-6} Torr vacuum. The exact result of this procedure is being investigated, however, we surmise that this treatment desorbs adsorbates from local heating[19]. A similar behavior was discovered on the other TMDs MoS_2, $MoSe_2$, and WSe_2[17] however WS_2 seems especially susceptible to this effect. Indeed a similar phenomenon was observed in a preliminary study of WS_2 where different charge states were accessed by varying the excitation power[20]. Therefore, while local desorption due to laser heating is the most likely mechanism, photo-desorption of adsorbates or possibly photo-doping are also possibilities. The free exciton is completely and reproducibly recovered when the sample is exposed to air, or some oxygen containing species (not, for instance nitrogen or helium). Using this technique, we isolate the trion from the free exciton, and create a reproducible initial condition.

Optical measurements.
We used a micro-Reflectivity/PL setup (spatial resolution of 1 μm) with a 50x objective, appropriate filters and incorporated a continuous-flow He-cryostat to collect reflectivity and PL in a backscattering geometry. Samples were excited with various continuous-wave lasers polarized as σ^+. Excitation energies are indicated where appropriate. Emitted light was dispersed by a single monochromator equipped with a multichannel CCD detector. The PL spectra were analyzed as σ^+ and σ^- using a combination of quarter-wave plate (liquid crystal) and linear polarizer placed before the spectrometer entrance slit. We obtain the same polarization when the sample is excited with negative helicity light, and have verified that peak intensity and peak area yield the same value for polarization. The emitted circular polarization is 0% when the sample is excited with linearly polarized light. The data at 4 K from the neutral exciton shown in Fig. 2 was taken with a power of 0.7 μW and integration time of 2 seconds. Because the intensity decreases exponentially as a function of temperature, significant signal could not be collected for the neutral exciton at elevated temperature while the sample was in vacuum.

Transport measurements.
Flakes were exfoliated onto SiO_2/n-Si substrates for the transport measurements. Top contacts were then deposited using standard e-beam lithographic techniques, and the n-Si was used as a global back gate. Channel resistance was monitored as a function of gate voltage to determine the sign of the charge carrier.

References

1. Gunawan, O. *et al.* Valley Susceptibility of an Interacting Two-Dimensional Electron System. *Phys. Rev. Lett.* **97,** 186404 (2006).
2. Rycerz, A., Tworzydło, J. & Beenakker, C. W. J. Valley filter and valley valve in graphene. *Nature Phys.* **3,** 172–175 (2007).
3. Xiao, D., Yao, W. & Niu, Q. Valley-Contrasting Physics in Graphene: Magnetic Moment and Topological Transport. *Phys. Rev. Lett.* **99,** 236809 (2007).
4. Xiao, D., Liu, G.-B., Feng, W., Xu, X. & Yao, W. Coupled Spin and Valley Physics in Monolayers of MoS_2 and Other Group-VI Dichalcogenides. *Phys. Rev. Lett.* **108,** 196802 (2012).
5. Cao, T. *et al.* Valley-selective circular dichroism of monolayer molybdenum disulphide. *Nat. Commun.* **3,** 887 (2012).
6. Mak, K. F., He, K., Shan, J. & Heinz, T. F. Control of valley polarization in monolayer MoS_2 by optical helicity. *Nat. Nanotechnol.* **7,** 494–498 (2012).
7. Yao, W., Xiao, D. & Niu, Q. Valley-dependent optoelectronics from inversion symmetry breaking. *Phys. Rev. B* **77,** 235406 (2008).
8. Zeng, H., Dai, J., Yao, W., Xiao, D. & Cui, X. Valley polarization in MoS_2 monolayers by optical pumping. *Nat. Nanotechnol.* **7,** 490–493 (2012).
9. Sallen, G. *et al.* Robust optical emission polarization in MoS_2 monolayers through selective valley excitation. *Phys. Rev. B* **86,** 081301R (2012).
10. Kioseoglou, G. *et al.* Valley polarization and intervalley scattering in monolayer MoS_2. *Appl. Phys. Lett.* **101,** 221907 (2012).
11. Jones, A. M. *et al.* Optical generation of excitonic valley coherence in monolayer WSe_2. *Nat. Nanotechnol.* **8,** 634–638 (2013).
12. Mai, C. *et al.* Exciton valley relaxation in a single layer of WS_2 measured by ultrafast spectroscopy. *Phys. Rev. B* **90,** 041414R (2014).
13. Lagarde, D. *et al.* Carrier and Polarization Dynamics in Monolayer MoS2. *Phys. Rev. Lett.* **112,** 047401 (2014).
14. Zhang, Y. J., Oka, T., Suzuki, R., Ye, J. T. & Iwasa, Y. Electrically Switchable Chiral Light-Emitting Transistor. *Science* **344,** 725–728 (2014).
15. Mak, K. F., McGill, K. L., Park, J. & McEuen, P. L. The valley Hall effect in MoS_2 transistors. *Science* **344,** 1489–1492 (2014).
16. Song, Y. & Dery, H. Transport Theory of Monolayer Transition-Metal Dichalcogenides through Symmetry. *Phys. Rev. Lett.* **111,** 026601 (2013).

17. Mak, K. F. *et al.* Tightly bound trions in monolayer MoS_2. *Nat. Mater.* **12,** 207–211 (2012).
18. Ross, J. S. *et al.* Electrical control of neutral and charged excitons in a monolayer semiconductor. *Nature Communications* **4,** 1474 (2013).
19. Currie, M., Hanbicki, A. T., Kioseoglou, G. & Jonker, B. T. Optical control of charged exciton states in tungsten disulfide. *Appl. Phys. Lett.* **106,** 201907 (2015).
20. Tongay, S. *et al.* Broad-Range Modulation of Light Emission in Two-Dimensional Semiconductors by Molecular Physisorption Gating. *Nano Lett.* **13,** 2831–2836 (2013).
21. Mitioglu, A. *et al.* Optical manipulation of the exciton charge state in single-layer tungsten disulfide. *Phys. Rev. B* **88,** 245403 (2013).
22. Shields, A. J., Pepper, M., Ritchie, D. A. & Simmons, M. Y. Influence of excess electrons and magnetic fields on Mott-Wannier excitons in GaAs quantum wells. *Adv. Phys.* **44,** 47–72 (1995).
23. Berkelbach, T. C., Hybertsen, M. S. & Reichman, D. R. Theory of neutral and charged excitons in monolayer transition metal dichalcogenides. *Phys. Rev. B* **88,** 045318 (2013).
24. He, K. *et al.* Tightly Bound Excitons in Monolayer WSe_2. *Phys. Rev. Lett.* **113,** 026803 (2014).
25. Chernikov, A. *et al.* Exciton Binding Energy and Nonhydrogenic Rydberg Series in Monolayer WS_2. *Phys. Rev. Lett.* **113,** 076802 (2014).
26. Ye, Z. *et al.* Probing excitonic dark states in single-layer tungsten disulphide. *Nature* **513,** 214–218 (2014).
27. Hanbicki, A. T., Currie, M., Kioseoglou, G., Friedman, A. L. & Jonker, B. T. Measurement of high exciton binding energy in the monolayer transition-metal dichalcogenides WS_2 and WSe_2. *Solid State Commun.* **203,** 16–20 (2015).
28. Zhu, B., Chen, X. & Cui, X. Exciton Binding Energy of Monolayer WS_2. *Sci. Rep.* **5,** 9218 (2015).
29. Solovyev, V. & Kukushkin, I. Measurement of binding energy of negatively charged excitons in $GaAs/Al_{0.3}Ga_{0.7}As$ quantum wells. *Phys. Rev. B* **79,** 233306 (2009).
30. Wang, G. *et al.* Polarization and time-resolved photoluminescence spectroscopy of excitons in $MoSe_2$ monolayers. *Appl. Phys. Lett.* **106,** 112101 (2015).
31. Molina-Sánchez, A. & Wirtz, L. Phonons in single-layer and few-layer MoS_2 and WS_2. *Phys. Rev. B* **84,** 205303 (2011).
32. Berkdemir, A. *et al.* Identification of individual and few layers of WS_2 using Raman Spectroscopy. *Sci. Rep.* **3,** 1755 (2013).
33. Wang, Q. *et al.* Valley Carrier Dynamics in Monolayer Molybdenum Disulfide from Helicity-Resolved Ultrafast Pump–Probe Spectroscopy. *ACS Nano* **7,** 11087–11093 (2013).
34. Mai, C. *et al.* Many-Body Effects in Valleytronics: Direct Measurement of Valley Lifetimes in Single-Layer MoS_2. *Nano Lett.* **14,** 202–206 (2014).
35. Yu, T. & Wu, M. W. Valley depolarization due to intervalley and intravalley electron-hole exchange interactions in monolayer MoS_2. *Phys. Rev. B* **89,** 205303 (2014).
36. Korn, T., Heydrich, S., Hirmer, M., Schmutzler, J. & Schüller, C. Low-temperature photocarrier dynamics in monolayer MoS_2. *Appl. Phys. Lett.* **99,** 102109 (2011).
37. Ye, Y. *et al.* Exciton-dominant electroluminescence from a diode of monolayer MoS_2. *Appl. Phys. Lett.* **104,** 193508 (2014).
38. Wang, H., Zhang, C. & Rana, F. Ultrafast Dynamics of Defect-Assisted Electron–Hole Recombination in Monolayer MoS_2. *Nano Lett.* **15,** 339–345 (2015).
39. Vaxenburg, R., Rodina, A., Shabaev, A., Lifshitz, E. & Efros, A. L. Nonradiative Auger Recombination in Semiconductor Nanocrystals. *Nano Lett.* **15,** 2092–2098 (2015).
40. Javaux, C. *et al.* Thermal activation of non-radiative Auger recombination in charged colloidal nanocrystals. *Nat. Nanotechnol.* **8,** 206–212 (2013).
41. Salehzadeh, O., Tran, N. H., Liu, X., Shih, I. & Mi, Z. Exciton Kinetics, Quantum Efficiency, and Efficiency Droop of Monolayer MoS_2 Light-Emitting Devices. *Nano Lett.* **14,** 4125–4130 (2014).
42. Palummo, M., Bernardi, M. & Grossman, J. C. Exciton Radiative Lifetimes in Two-Dimensional Transition Metal Dichalcogenides. *Nano Lett.* **15,** 2794–2800 (2015).

Acknowledgements

Author Contributions

A.H., G.K. and M.C. performed the experiments. A.H., G.K., M.C. and C.S.H. analyzed the data. A.F. performed transport measurements. A.F. and K.M.M. provided samples. All authors discussed the results and contributed to the manuscript.

Additional Information

Supplementary information accompanies this paper at http://www.nature.com/srep

Competing financial interests: The authors declare no competing financial interests.

How to cite this article: Hanbicki, A.T. *et al.* Anomalous temperature-dependent spin-valley polarization in monolayer WS_2. *Sci. Rep.* **6,** 18885; doi: 10.1038/srep18885 (2016).